

# A METHOD FOR ACCURATE MEASUREMENT OF HELIOSTAT MIRROR ORIENTATION

**Benjamin D. Swart<sup>1</sup>, Herman A. Engelbrecht<sup>2</sup>, and Johann Treurnicht<sup>3</sup>**

<sup>1</sup> Solar Thermal Energy Research Group, Department of Mechanical and Mechatronic Engineering, Stellenbosch University, Private Bag X1, Matieland, 7602, South Africa; Phone: +27 21 808 4016; Fax: +27 21 808 4933; E-Mail: bdsward@sun.ac.za

<sup>2</sup> MIH Media Lab, Stellenbosch University; E-Mail: hebrecht@sun.ac.za

<sup>3</sup> Stellenbosch University; E-mail: jtreurn@sun.ac.za

## Abstract

A method is developed for the measurement of the mirror orientations of all heliostats in a field simultaneously. Tower mounted electromagnetic transmitters are placed at known positions around the perimeter of the heliostat field, transmitting identical sinusoidal signals. An electromagnetic receiver in the field uses a Hilbert transform-based method to calculate the phase difference between a pair of signals, and using the wavelength, calculates the difference in distance between itself and the corresponding pair of transmitters. The receiver position is then approximated using multilateration with a non-linear least squares algorithm. By attaching three receivers to the heliostat mirror surface at distinct points, a plane parallel to the mirror surface is formed which is used to determine the mirror orientation. A simulation of the system implementing the proposed method is constructed to verify that the method works, and results show that for the error sources included in the model it is theoretically possible to achieve a tracking error of one milliradian or less.

*Keywords: Heliostat; tracking; closed-loop; orientation.*

## 1. Introduction

The central receiver system (CRS) is a relatively new technology within the field of concentrating solar power (CSP) and predictions indicate significant opportunities to reduce the levelised cost of electricity (LCOE) by as much as 40% from 2010 to 2020 [1] by increasing performance and lowering costs. The performance of CRS plants is highly dependent on the efficiency of the heliostat field, which in itself contributes an estimated 30% - 50% of the total plant cost [2] [3].

Heliostat field efficiency is increased by reflecting a greater

portion of the solar radiation incident on the field onto the receiver. This typically requires an increased accuracy in heliostat tracking. Open-loop tracking is hindered by problems such as mechanical tolerances, while current closed-loop tracking methods are either impractical, not accurate enough, or too expensive [4] [5] [6] [7]. The current industry norm seems to be open-loop tracking using an error model [8] for a tracking error of less than one milliradian. This, however, requires periodic recalibration of error parameters which can take up to three weeks for the entire field [9] [10].

This paper investigates heliostat mirror orientation as a possible source of feedback for closed-loop tracking systems. A method is developed to accurately determine the mirror orientations of all heliostats simultaneously with an accuracy that aims to match or exceed current standards. The concept for such a system is developed in the following section, after which some of the core aspects are developed in detail. The results demonstrate a working simulation of the system and investigate the effects of some error sources on its performance. The paper is concluded with some final remarks.

## 2. Conceptual Overview of Proposed System

In the past, sites such as Solar One have used inclinometers to measure the heliostat azimuth axis tilt angle [11]. While such methods can certainly be used to further improve results, they are not the focus of this paper. Instead, this paper focuses on an approach where the heliostat orientation is obtained by accurately measuring the coordinates of three or more distinct points on its mirror surface. These points define a plane which, when parallel to the mirror, is used to calculate the heliostat normal vector. For simplicity, it is assumed in this paper that the plane and mirror surface are parallel, though it is possible to develop an error model to compensate for any non-parallelism.

The approach for determining the coordinates of a single point within a predetermined three-dimensional space is based on a 2007 master's thesis by Murphy [12] which addresses a similar problem. Electromagnetic receivers are placed at three or more points on the mirror surface for which the coordinates are required. Tower mounted transmitters are placed at known positions around the perimeter of the heliostat field as shown in Fig. 1. A single central oscillator is connected to each transmitter to ensure that all transmitters transmit a sinusoidal signal of exactly the same frequency, though the phases may differ. The distance  $d_i$  between a receiver and transmitter  $T_i$  results in a phase shift of  $\phi_i$  from the time the signal is transmitted to the time it is received. While measuring  $\phi_i$  may prove problematic, it is possible to measure the difference in phase shift  $\phi_i - \phi_j$  between two signals (§3.1) from transmitters  $T_i$  and  $T_j$ . This value is proportional to  $d_i - d_j$ , the distance between the receiver and transmitter  $T_i$  relative to the distance between the receiver and transmitter  $T_j$ . When the wavelength, and thus frequency, of the sinusoid is known,  $d_i - d_j$  can be calculated exactly (§3.2). These measured distance differences, along with the known positions of the transmitters (§3.3), are then used in an algorithm using multilateration and non-linear least squares to calculate the position of the receiver (§3.4). When the positions of all receivers on the mirror surface have been calculated, the corresponding plane and resulting normal vector is calculated (§3.5). This process is illustrated in Fig. 2.

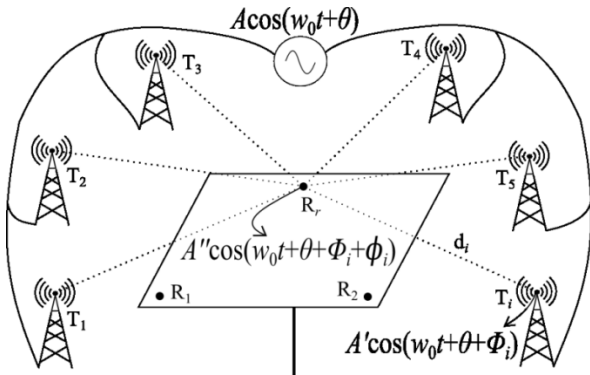


**Fig. 1 Conceptual illustration of transmitter towers surrounding heliostat field.**

Even though the frequency of all transmitted signals is the same, each signal undergoes a different phase shift  $\phi_i$  from the time it is generated at the central oscillator to the time it is transmitted at  $T_i$ . These values may change slowly throughout the day and need to be periodically recalculated. This is done by placing a calibration receiver at a known position within the field which uses its own position, the known positions of the transmitters, and the expected phase shift due to the known distance  $d_i$  to calculate the value of  $\phi_i$  for each  $T_i$  (§3.6).

Transmitters use frequency division multiplexing (FDM) for concurrent transmission of all signals over the shared medium (air). That is, each transmitter  $T_i$  modulates the sinusoidal signal onto a unique carrier frequency which allows a receiver to demodulate the received signals and, based on the carrier frequency, determine which  $T_i$  each signal originated from.

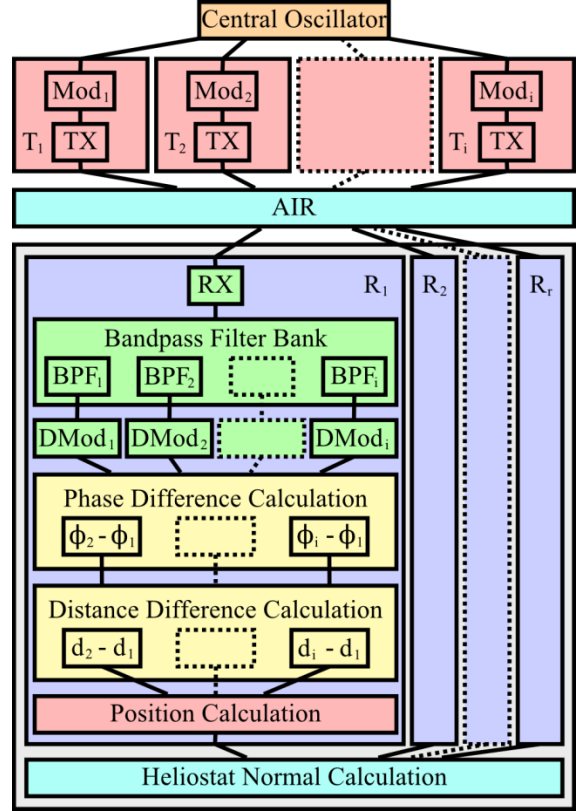


**Fig. 2 Overview of process leading to calculation of heliostat mirror normal vector. RX and TX represent electromagnetic transmitters and receivers, and  $Mod_i$  and  $DMod_i$  represent modulators and demodulators for the carrier frequency of transmitter  $T_i$ .**

### 3. Development of Core Aspects

#### 3.1. Phase Difference Calculation

Three methods are considered for the calculation of phase difference between two sinusoids of matching frequency: dot product, dot product with noise compensation, and the Hilbert transform. Omitted methods include the discrete Fourier transform due to the problem of spectral leakage, and cross correlation due to the maximum achievable accuracy being limited by sampling frequency. The two signals are defined as

$$s_1(t) = a_1 \cos(\omega_0 t + \phi_1(t)) + n_1(t)$$

$$s_2(t) = a_2 \cos(\omega_0 t + \phi_2(t)) + n_2(t),$$

where  $n_1(t)$  and  $n_2(t)$  are ergodic random variables representing noise that is uncorrelated with the sinusoids.

### 3.1.1. Dot Product

One of the simplest ways to calculate the phase difference between two sinusoids is by using the dot product. Let  $\vec{s}_1$  be a vector containing  $S$  samples from  $s_1(t)$  sampled at a frequency of  $1/T$ , where the  $i$ th sample is given by

$$\vec{s}_1[i] = s_1(iT), \quad 0 \leq i \leq S-1,$$

and let  $\vec{s}_2$  be given similarly. When  $\phi_1(t)$  and  $\phi_2(t)$  remain constant, then it follows from the dot product that

$$\vec{s}_1 \cdot \vec{s}_2 = \|\vec{s}_1\| \|\vec{s}_2\| \cos(\phi_{21}),$$

where  $\|\vec{s}_1\|$  and  $\|\vec{s}_2\|$  denote the sizes of vectors  $\vec{s}_1$  and  $\vec{s}_2$ , respectively, and  $\phi_{21}$  is the phase difference between the two sinusoids. The equation is solved for  $\phi_{21}$  as follows:

$$\phi_{21} = |\phi_2 - \phi_1| = \text{acos}\left(\frac{\vec{s}_1 \cdot \vec{s}_2}{\|\vec{s}_1\| \|\vec{s}_2\|}\right).$$

### 3.1.2. Dot Product with Noise Compensation

One shortcoming of the dot product method is that it does not account for noise. When the mean  $E[n]$  and variance  $\text{Var}[n]$  of the noise is known, it is possible to compensate for the effect of noise on the calculated phase difference.

Multiplication of  $s_1(t)$  and  $s_2(t)$  yields

$$\begin{aligned} s(t) &= [s_1(t)][s_2(t)] \\ &= \frac{a_1 a_2}{2} \cos(\phi_2 - \phi_1) + \frac{a_1 a_2}{2} \cos(2\omega_0 t + \phi_2 + \phi_1) \\ &\quad + a_1 \cos(\omega_0 t + \phi_1) n_2(t) \\ &\quad + a_2 \cos(\omega_0 t + \phi_2) n_1(t) + n_1(t)n_2(t). \end{aligned}$$

The mean of the signal  $s(t)$  is calculated as

$$s_u = \frac{1}{T} \int_0^T s(t) dt = \frac{a_1 a_2}{2} \cos(\phi_2 - \phi_1) + E[n_1 n_2],$$

which follows from the fact that the mean of the periodic terms approach zero as  $T$  becomes sufficiently large, and where  $E[n_1 n_2]$  is the expected value (mean) of the product of  $n_1$  and  $n_2$ . Rearranging the terms gives the phase difference as

$$\phi_{21} = |\phi_2 - \phi_1| = \text{acos}\left(\frac{2(s_u - E[n_1 n_2])}{a_1 a_2}\right).$$

The amplitudes of the original signals,  $a_1$  and  $a_2$ , are calculated by multiplying the original signal by itself, taking the average, and then rearranging the terms:

$$[s_1(t)]_u^2 = \frac{1}{T} \int_0^T [s_1(t)]^2 dt = \frac{a_1^2}{2} + E[n_1^2],$$

from which it follows that

$$a_1 = \sqrt{2([s_1(t)]_u^2 - E[n_1^2])}, \quad E[n_1^2] = \text{Var}[n_1] + E[n_1]^2,$$

where  $\text{Var}[n_1]$  is the variance of  $n_1$ . The value of  $a_2$  is calculated similarly. By letting  $u_{12} = E[n_1 n_2]$ ,  $u_1 = E[n_1]$ ,  $u_2 = E[n_2]$ ,  $\sigma_1^2 = \text{Var}[n_1]$ , and  $\sigma_2^2 = \text{Var}[n_2]$ , the final equation for the phase difference becomes

$$\phi_{21} = \text{acos}\left(\frac{s_u - u_{12}}{\sqrt{([s_1(t)]_u^2 - \sigma_1^2 - u_1^2)([s_2(t)]_u^2 - \sigma_2^2 - u_2^2)}}\right).$$

It is important to note that neither this nor the previous method includes the sign of the angle  $\phi_{21}$ .

### 3.1.3. Hilbert Transform

Let  $\hat{s}_1(t)$  and  $\hat{s}_2(t)$  denote the Hilbert transforms of  $s_1(t)$  and  $s_2(t)$ , respectively, given by

$$\hat{s}_1(t) = a_1 \sin(\omega_0 t + \phi_1(t)) + \hat{n}_1(t)$$

$$\hat{s}_2(t) = a_2 \sin(\omega_0 t + \phi_2(t)) + \hat{n}_2(t),$$

and let  $h_1(t)$  and  $h_2(t)$  be the positive analytical signals

$$h_1(t) = s_1(t) + j\hat{s}_1(t), \quad h_2(t) = s_2(t) + j\hat{s}_2(t).$$

The analytical signals can be viewed as rotating vectors with angle  $\Theta(t) = \omega_0 t + \phi(t) + \gamma(t)$ , where  $\gamma(t)$  is the variation in phase due to noise. The angle  $\Theta$  of a complex signal  $h$  is

$$\Theta = \arg(h) = \text{atan2}(\text{imag}(h), \text{real}(h)),$$

which leads to the difference in angle between two complex signals  $h_1(t)$  and  $h_2(t)$  being calculated as

$$\begin{aligned} \Theta_2(t) - \Theta_1(t) &= \phi_2(t) - \phi_1(t) + \gamma_2(t) - \gamma_1(t) \\ &= \text{atan2}(\hat{s}_2(t), s_2(t)) - \text{atan2}(\hat{s}_1(t), s_1(t)). \end{aligned}$$

When the signal-to-noise ratio is large enough,

$$\gamma_2(t) - \gamma_1(t) \approx 0,$$

$$\phi_2(t) - \phi_1(t) = \text{atan2}(\hat{s}_2(t), s_2(t)) - \text{atan2}(\hat{s}_1(t), s_1(t)).$$

Additionally, if the phase difference is assumed to be constant, the accuracy of the results can be improved by averaging over time. Using phasor geometry to account for phase wrapping, the averages of the real and imaginary components of the phase difference are calculated as

$$\begin{aligned} x &= \frac{1}{T} \int_0^T \cos(\phi_2(t) - \phi_1(t)) dt \\ y &= \frac{1}{T} \int_0^T \sin(\phi_2(t) - \phi_1(t)) dt. \end{aligned}$$

The resulting phase difference, averaged over time, is then

$$\phi_{21} = \phi_2 - \phi_1 = \text{atan}(y, x).$$

### 3.2. Translating Phase Difference to Distance

A phase difference  $\phi_i - \phi_j \in (-\pi, \pi]$  between two sinusoids with matching frequency and wavelength  $\lambda$  is translated into distance by the equation

$$d_i - d_j = -\left(\frac{\phi_i - \phi_j - (\Phi_i - \Phi_j)}{2\pi}\right)\lambda + n\lambda,$$

where  $d_i - d_j$  represents the distance between the receiver and transmitter  $T_i$  relative to the distance between the receiver and transmitter  $T_j$ . A negative value of  $\phi_i - \phi_j$  indicates that  $T_j$  is further away than  $T_i$ , hence the minus prefix.

The  $n\lambda$  term indicates that any number of full wavelengths may be added to the result due to the periodic nature of a sinusoidal wave. For example, a distance of  $\lambda/4$  and  $5\lambda/4$  will both yield a phase difference of  $\pi/2$ . When the position of the receiver is approximately known, the correct value of  $n$  can be substituted into the equation. Another solution is to transmit more than one sinusoid such that the sinusoid with a longer wavelength is used to approximate while the sinusoid with a shorter wavelength is used to accurately determine the receiver position. In this paper it is assumed that the wavelength  $\lambda$  is longer than the diameter of the field such that  $n$  is always zero.

### 3.3. Transmitter Layout

There are many factors to consider for the optimal layout of transmitter towers. Examples of such factors include the distances between transmitters and receivers (greater distances require higher signal power) and line of sight (the changing orientation of a heliostat limits the set of transmitters it has line of sight to). Taking into account all possible factors is a study in its own right. The only factor considered here is the sensitivity of the transmitter geometry to noise.

### 3.4. Position Calculation

The calculated position  $\hat{R}$  of a receiver at  $R$  is determined using multilateration. Let there be  $N$  transmitters located at known positions  $T_i$ , with the distance between each  $T_i$  and  $R$  given by  $d_i$ , and the distance between each  $T_i$  and  $\hat{R}$  given by  $\hat{d}_i$ . Due to noise and other factors, a small error  $\epsilon_i = \hat{d}_i - d_i$  exists, which is minimised using a non-linear least squares algorithm.

When  $d_i$  is measured relative to a reference distance  $d_r$  instead of being an absolute measurement, then  $d_i = d_r + \Delta_i$ , where  $d_r$  is the reference distance and  $\Delta_i$  is the difference between  $d_i$  and  $d_r$ . When relative distances are used,  $N \geq D + 2$ , where  $D$  is the number of dimensions. For three dimensions,  $N \geq 5$ .

The error function is properly defined as

$$\begin{aligned} \epsilon_i(x, y, z) &= \hat{d}_i - d_i \\ &= \sqrt{(x - T_{i,x})^2 + (y - T_{i,y})^2 + (z - T_{i,z})^2} - (d_r + \Delta_i), \end{aligned}$$

where  $x$ ,  $y$  and  $z$  are the calculated position of the receiver  $\hat{R}$ .

The goal is to minimise the sum of the squares of the errors

$$E(x, y, z) = \sum_{i=1}^N \epsilon_i(x, y, z)^2.$$

Differentiating  $E$  with respect to  $x$  yields

$$\frac{\partial E}{\partial x} = 2 \sum_{i=1}^N \epsilon_i \frac{\partial \epsilon_i}{\partial x}$$

with  $\partial E/\partial y$ ,  $\partial E/\partial z$  and  $\partial E/\partial d_r$  obtained similarly. The derivative of  $\epsilon_i$  with respect to  $x$  is given by

$$\frac{\partial \epsilon_i}{\partial x} = \frac{x - T_{i,x}}{\sqrt{(x - T_{i,x})^2 + (y - T_{i,y})^2 + (z - T_{i,z})^2}} = \frac{x - T_{i,x}}{\epsilon_i + d_r + \Delta_i}$$

with  $\partial \epsilon_i/\partial y$ ,  $\partial \epsilon_i/\partial z$  obtained similarly, and  $\partial \epsilon_i/\partial d_r = -1$ .

Introducing the vectors  $\vec{\epsilon}$ ,  $\vec{g}$  and the Jacobian matrix  $\mathbf{J}$ , leads to

$$\vec{g} = 2\mathbf{J}^T \vec{\epsilon},$$

$$\vec{g} = \begin{bmatrix} \frac{\partial E}{\partial x} \\ \frac{\partial E}{\partial y} \\ \frac{\partial E}{\partial z} \\ \frac{\partial E}{\partial d_r} \end{bmatrix}, \quad \mathbf{J} = \begin{bmatrix} \frac{\partial \epsilon_1}{\partial x} & \frac{\partial \epsilon_1}{\partial y} & \frac{\partial \epsilon_1}{\partial z} & \frac{\partial \epsilon_1}{\partial d_r} \\ \frac{\partial \epsilon_2}{\partial x} & \frac{\partial \epsilon_2}{\partial y} & \frac{\partial \epsilon_2}{\partial z} & \frac{\partial \epsilon_2}{\partial d_r} \\ \vdots & \vdots & \vdots & \vdots \\ \frac{\partial \epsilon_N}{\partial x} & \frac{\partial \epsilon_N}{\partial y} & \frac{\partial \epsilon_N}{\partial z} & \frac{\partial \epsilon_N}{\partial d_r} \end{bmatrix}, \quad \vec{\epsilon} = \begin{bmatrix} \epsilon_1 \\ \vdots \\ \epsilon_N \end{bmatrix}.$$

Using the vector

$$\vec{\beta} = [x \quad y \quad z \quad d_r]^T,$$

where  $x$ ,  $y$  and  $z$  are the calculated position of  $\hat{R}$ , Newton iteration gives

$$\vec{\beta}_{k+1} = \vec{\beta}_k - (\mathbf{J}_k^T \mathbf{J}_k)^{-1} \mathbf{J}_k^T \vec{\epsilon}_k,$$

where  $\vec{\beta}_k$  denotes the  $k^{\text{th}}$  approximate solution. The subscript  $k$  in  $\mathbf{J}$  and  $\vec{\epsilon}$  means that these quantities are evaluated at  $\vec{\beta}_k$ . Also given is

$$\mathbf{J}^T \mathbf{J} = \begin{bmatrix} \sum_{i=1}^N \frac{(x - T_{i,x})^2}{(\epsilon_i + d_r + \Delta_i)^2} & \sum_{i=1}^N \frac{(x - T_{i,x})(y - T_{i,y})}{(\epsilon_i + d_r + \Delta_i)^2} \\ \sum_{i=1}^N \frac{(x - T_{i,x})(y - T_{i,y})}{(\epsilon_i + d_r + \Delta_i)^2} & \sum_{i=1}^N \frac{(y - T_{i,y})^2}{(\epsilon_i + d_r + \Delta_i)^2} \\ \sum_{i=1}^N \frac{(x - T_{i,x})(z - T_{i,z})}{(\epsilon_i + d_r + \Delta_i)^2} & \sum_{i=1}^N \frac{(y - T_{i,y})(z - T_{i,z})}{(\epsilon_i + d_r + \Delta_i)^2} \\ \sum_{i=1}^N \frac{-(x - T_{i,x})}{\epsilon_i + d_r + \Delta_i} & \sum_{i=1}^N \frac{-(y - T_{i,y})}{\epsilon_i + d_r + \Delta_i} \\ \sum_{i=1}^N \frac{(x - T_{i,x})(z - T_{i,z})}{(\epsilon_i + d_r + \Delta_i)^2} & \sum_{i=1}^N \frac{-(x - T_{i,x})}{\epsilon_i + d_r + \Delta_i} \\ \sum_{i=1}^N \frac{(y - T_{i,y})(z - T_{i,z})}{(\epsilon_i + d_r + \Delta_i)^2} & \sum_{i=1}^N \frac{-(y - T_{i,y})}{\epsilon_i + d_r + \Delta_i} \\ \sum_{i=1}^N \frac{(z - T_{i,z})^2}{(\epsilon_i + d_r + \Delta_i)^2} & \sum_{i=1}^N \frac{-(z - T_{i,z})}{\epsilon_i + d_r + \Delta_i} \\ \sum_{i=1}^N \frac{-(z - T_{i,z})}{\epsilon_i + d_r + \Delta_i} & \sum_{i=1}^N 1 \end{bmatrix},$$

$$\mathbf{J}^T \vec{\epsilon} = \begin{bmatrix} \sum_{i=1}^N \frac{x - T_{i,x}}{\epsilon_i + d_r + \Delta_i} \epsilon_i & \sum_{i=1}^N \frac{y - T_{i,y}}{\epsilon_i + d_r + \Delta_i} \epsilon_i \\ \sum_{i=1}^N \frac{z - T_{i,z}}{\epsilon_i + d_r + \Delta_i} \epsilon_i & \sum_{i=1}^N -\epsilon_i \end{bmatrix}^T.$$

### 3.5. Receiver Plane Normal Vector

When the positions of three points ( $R_1, R_2, R_3$ ) on the mirror plane are known, the unit vector  $\vec{u}$  normal to the plane is calculated using the cross product as

$$\vec{v} = (R_2 - R_1) \times (R_3 - R_1), \quad \vec{u} = \frac{\vec{v}}{\|\vec{v}\|}$$

When the receivers are numerically arranged counter-clockwise as viewed from the front, then  $\vec{u}$  is in the forward facing direction of the heliostat, otherwise it is backwards.

### 3.6. Electronic Phase Delay Calculation

The calibration receiver at  $R_c$  calculates the phase differences of the signals it receives in exactly the same way as any other receiver does. The value of the phase shift  $\Phi_i$  from the central oscillator to transmitter  $T_i$  is then equal to the sum of the expected phase shift due to the receiver's distance from  $T_i$  and the measured phase difference  $\phi_i$ :

$$d_i = \sqrt{(T_{i,x} - R_{c,x})^2 + (T_{i,y} - R_{c,y})^2 + (T_{i,z} - R_{c,z})^2},$$

$$\Phi_i = \frac{2\pi d_i}{\lambda} + \phi_i.$$

The value of  $\Phi_i$  is wrapped to fit in the range  $(-\pi, \pi]$ .

## 4. Results

### 4.1. Phase Difference Calculation

Fig. 3, Fig. 4 and Fig. 5 show the accuracy with which the phase difference between two sinusoids of matching frequency can be calculated using the methods described in section 3.1. All simulations assume zero-mean noise with constant power spectral density (PSD). The signal-to-noise ratio (SNR) is indicated on the x-axis and the standard deviation of the error is indicated on the y-axis in degrees. The SNR is the same for both signals, except where indicated otherwise. Table 1 clarifies the legend used in the figures.

Key	Meaning
S	Number of samples.
SPC	Samples per cycle, which is a measure of the normalised sampling frequency.
B	Equivalent normalised noise bandwidth. No filtering is indicated by 'none'.
SNR2	Indicates that the SNR of the second signal is SNR2-times more than the SNR of the first signal.

**Table 1 Clarification of the legends for Figures 3, 4 and 5.**

Recall that of the three methods investigated, only the Hilbert Transform method correctly includes the sign of the angle  $\phi_{21}$ . It therefore only makes sense to record the absolute value of the error for the other two methods, which would inevitably introduce a positive non-zero bias in the error mean. This makes comparison difficult and is avoided by assuming the

correct sign for  $\phi_{21}$  in the simulation for these methods.

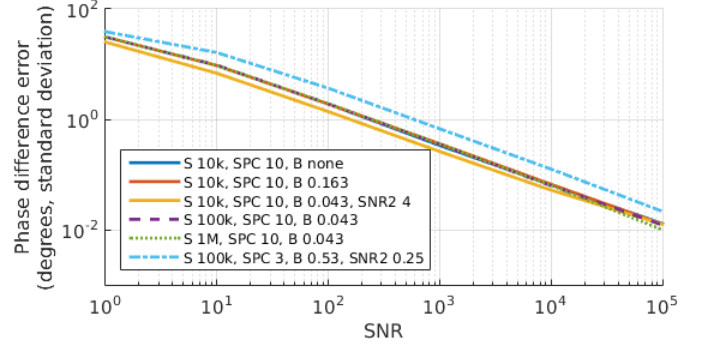


**Fig. 3 Performance of Dot Product method.**

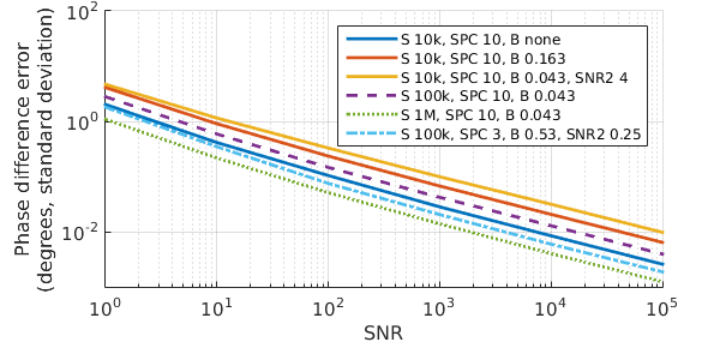


**Fig. 4 Performance of Dot Product with Noise Compensation method.**

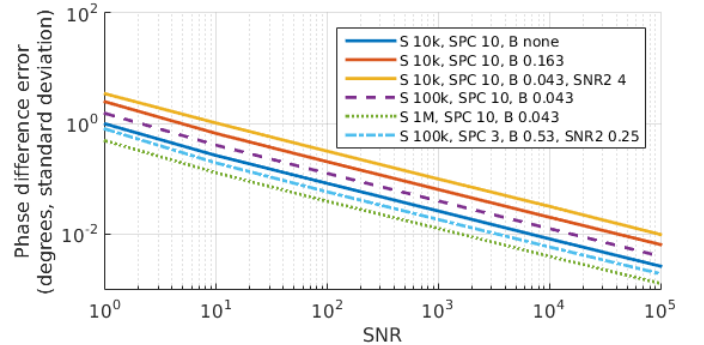


**Fig. 5 Performance of Hilbert Transform method.**

The resulting error mean for all graphs is approximately zero (mean  $\ll$  standard deviation) so the standard deviation of the error is used as the metric to compare results. All figures clearly show a decrease in the resulting phase difference error as the SNR is increased. Fig. 3 shows that the sampling frequency, number of samples and filter bandwidth have little to no effect on the results of the first method. For the latter two methods, however, it is clear from Fig. 4 and Fig. 5 that an increase in the number of samples as well as a wider bandwidth (while maintaining the same SNR, thus lower PSD) both contribute towards a smaller error. As expected, the accuracy of the dot product method is significantly increased when noise compensation is added, to the point where it is almost identical

to the accuracy of the Hilbert transform method. Keep in mind, however, that the former requires the noise characteristics to be exactly known, whereas the latter has no such requirement. The results in Fig. 4 quickly approach those of Fig. 3 (or worse) when the noise characterisation contains errors. Fig. 6 shows how the accuracy of the Hilbert transform method is independent of the phase difference, whereas the other methods are more sensitive to noise at certain phase differences. The Hilbert transform is clearly superior to the other methods.

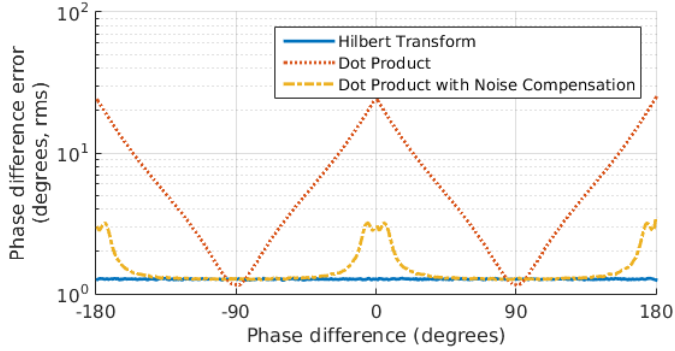


**Fig. 6 Sensitivity of methods at various phase differences with SNR = 10.**

#### 4.2. Transmitter Layout

The placement of transmitter towers plays an important part in the overall accuracy of the system. Poor transmitter placement can result in large receiver position errors even when phase difference errors are small. From experimentation with the layout of transmitter towers the following guidelines for their optimal placement emerge:

- Any two transmitters should not be placed close to or on the same location.
- Any three transmitters should not be placed close to or on the same line.
- Any four transmitters should not be placed close to or on the same plane.
- Transmitters should surround and be placed outside the field of receivers, not within.

The last guideline is especially important when working with relative distances as the error rapidly increases once a receiver is outside the enclosure of transmitters as shown in Fig. 7. The optimal layout of transmitters in two dimensions is equally distributed on a circle surrounding the field of receivers. For three dimensions, the optimal layout is equally distributed on a sphere surrounding the field of receivers. Fig. 7 shows how the error on the receiver position is affected by varying the number of transmitters and the error on the measured distances. An optimal layout for two dimensions is used for simplicity and transmitters are equally distributed on a circle with normalised

radius of unity. It is evident that an increased number of transmitters as well as an increased accuracy in the measurement of the distances both contribute to a smaller error in receiver position.

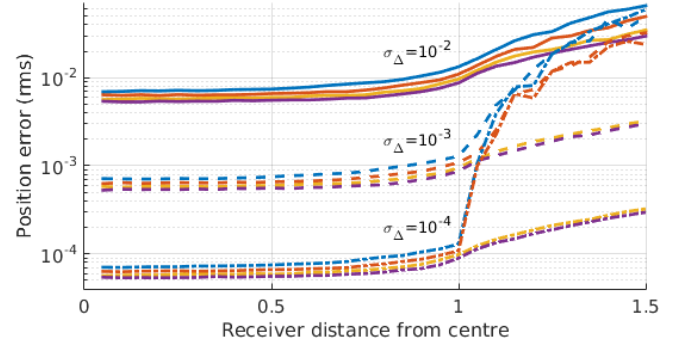


**Fig. 7 Receiver position error as affected by number of transmitters and error on measured distances. The number of transmitters is 4 (blue), 5 (red), 6 (orange) and 7 (purple).**

For practical reasons an ideal layout may not always be possible. One such constraint is the maximum possible height of a transmitter tower. The transmitter layout used in the remainder of this paper is shown in Fig. 8 and described in Table 2. Note that this does not necessarily represent an optimal layout as transmitter positions are constrained by both a minimum and a maximum height. The layout represents a flattened, elevated dome above the heliostat field. Coordinates are normalised to a field with radius of unity to enable the prediction of results for a larger field by simply scaling the normalised results. The performance of this layout is analysed in the following section.

TX #	X	Y	Z
1	1	0	0.2
2	0.5	0.866	0.3
3	-0.5	0.866	0.2
4	-1	0	0.3
5	-0.5	-0.866	0.2
6	0.5	-0.866	0.3
7	0.433	0.25	0.4
8	-0.433	0.25	0.4
9	0	-0.5	0.4
10	0	0	0.5

**Table 2 Normalised coordinates for transmitter layout.**

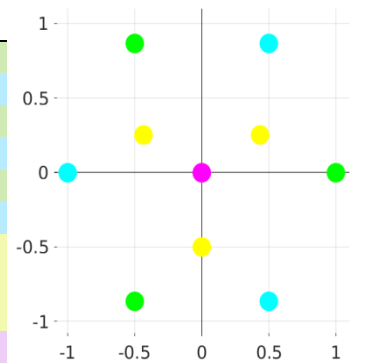


**Fig. 8 Top view of transmitter layout. Colours correlate to height.**

#### 4.3. Position Calculation

The simulated receiver position error for the transmitter layout proposed in Table 2 is shown in Fig. 9. The results show that for the proposed layout, an error on the distance measurement ( $\sigma_\Delta$ ) will result in a position RMS error  $\epsilon_R$  of  $0.99\sigma_\Delta$  at the

centre of the field and  $1.85\sigma_\Delta$  at the edge. The error at the edge of the field can be reduced by increasing the transmitter radius, while the overall error can be reduced by adding more transmitters and optimising the transmitter layout.

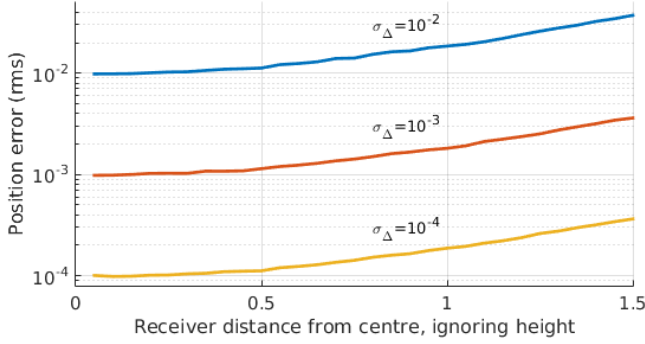


**Fig. 9 Receiver position error for proposed transmitter layout in Table 2 for varying error on measured distances.**

#### 4.4. Receiver Plane Normal Vector

Fig. 10 shows how the accuracy with which the receiver plane normal can be determined is affected by errors in the estimated receiver positions. Three receivers, all a distance  $d_R$  apart, form the receiver plane and the RMS error in each receiver position is  $\epsilon_R$ . The relationship  $d_R/\epsilon_R$  is shown on the x-axis, with the resulting error of the plane normal on the y-axis. Fig. 10 shows clearly that the plane normal error decreases as  $d_R/\epsilon_R$  increases, that is, as either the position error decreases or the receivers are placed a greater distance apart. From Fig. 10, the RMS of the tracking error  $T_{RMS}$  is approximated by

$$T_{RMS} = (1000\sqrt{4/3}) \frac{\epsilon_R}{d_R},$$

where  $T_{RMS}$  represents the overall tracking accuracy of the system, in milliradians. For a tracking error of less than one milliradian, a  $d_R/\epsilon_R$  relationship of above  $\sim 1150$  is required. The results assume that the receiver position errors are uncorrelated, though it can be shown that a positive correlation leads to a smaller RMS tracking error  $T_{RMS}$  for the same  $d_R/\epsilon_R$ .

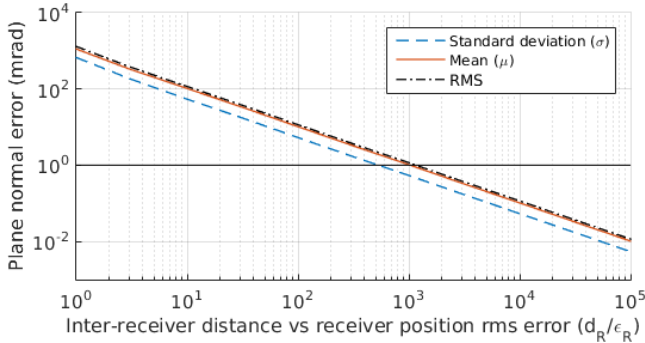


**Fig. 10 Receiver plane normal error as a function of receiver position error and inter-receiver distance.**

#### 4.5. Overall

The combined performance of all the previously discussed components is shown in Fig. 11 with the system parameters in the caption. The figure shows that an RMS tracking error of less than 10 milliradians is achievable with 100k samples and that the error approaches the 1 milliradian mark as the number of samples is increased. The maximum value shown for  $S$  is  $10^6$  samples, though this number can be increased until the desired accuracy is achieved.

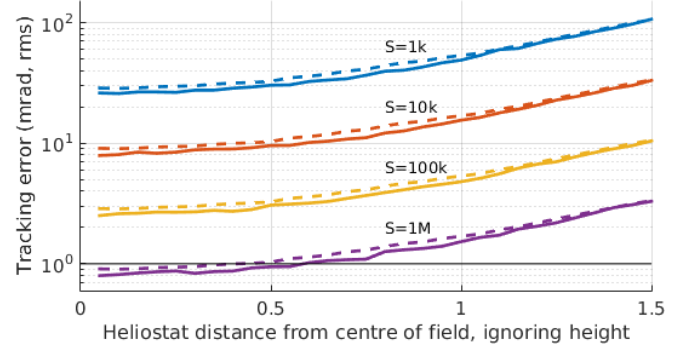


**Fig. 11 Overall tracking error with transmitters as in Table 2.  $SPC = 10$ ,  $SNR = 10^5$ ,  $B = 0.04$ ,  $\lambda = 4$ ,  $d_R = 0.0173$ . Simulated graphs are solid and predictions are dashed.**

The above figure also shows the accuracy with which the final error can be predicted, given the error of the individual components and the system parameters. The equation that accurately describes the variance of the error of the Hilbert transform method shown in Fig. 5 is given by

$$\sigma_\phi^2 = \frac{1}{S} \left( \frac{1}{B_1(SNR_1)} + \frac{1}{B_2(SNR_2)} \right),$$

where  $S$  is the number of samples,  $B_i$  is the equivalent normalised noise bandwidth ( $\times \sim 2/f_s$ ) of signal  $i$  with sampling frequency  $f_s$ , and  $SNR_i$  is the signal to noise ratio of signal  $i$ . With the given parameters and  $S = 10^6$  samples, the tracking error at the edge of the field is predicted by calculating the phase difference error variance  $\sigma_\phi^2 = 4.65 \times 10^{-10}$ , giving a distance difference error variance  $\sigma_\Delta^2 = (\lambda/2\pi)^2 \sigma_\phi^2 = 1.89 \times 10^{-10}$ , giving a position RMS error of  $\epsilon_R = 1.85\sigma_\Delta = 2.54 \times 10^{-5}$ , so that  $d_R/\epsilon_R = 682$  which results in a tracking RMS error of  $T_{RMS} = 1000\sqrt{4/3}\epsilon_R/d_R = 1.69$  milliradians. The difference between the predicted and simulated results is due to a small positive correlation in the simulated receiver position errors which reduces the tracking error. The same results can be applied to a larger field by scaling the transmitter coordinates in Table 2, signal wavelength  $\lambda$  and inter-receiver distance  $d_R$  by a factor  $x$ . For example if  $x = 100$ , then each transmitter coordinate is multiplied by  $x$  such that the field radius is 100,  $\lambda = 400$ , and  $d_R = 1.73$ .

## 5. Conclusion

The results in the previous section show that the most important factors for an increased tracking accuracy are an increased number of samples  $S$ , an increased signal-to-noise ratio  $SNR$ , a smaller wavelength  $\lambda$ , and a larger inter-receiver distance  $d_R$ . The importance of transmitter placement is also shown. A properly optimised transmitter layout will result in an even smaller tracking error.

A larger  $d_R$  favours larger heliostats over smaller ones. Since heliostats need to update their orientations multiple times per minute, a higher sampling rate is favourable as it will yield a larger number of samples within the allotted time. Using multiple wavelengths to approximate and pinpoint receiver positions introduces additional complexity but offers considerable increases in accuracy. Increasing the number of transmitters also increases accuracy, albeit only marginally.

While this paper focuses mainly on one of the unavoidable error sources, namely phase difference error due to noise, other possible error sources also exist, such as errors in the electronic phase delay  $\Phi$ , errors in the transmitter positions, and other hardware-specific errors, the effects of which will most certainly lead to an increased tracking error.

From a financial viewpoint the proposed method offers significant advantages. While the required infrastructure may be expensive, it is also minimal: only the central oscillator and transmitter towers. The important consideration is the added cost per heliostat. This amounts to only the three electromagnetic receivers, some electronics, and a processing unit, which in most cases is already present.

In the case where the time between heliostat orientation updates limits the number of samples to such an extent that a tracking error of less than one milliradian is unachievable, the system may become unsuitable for real-time use. It can, however, still be used to aid in the calibration process. The orientation of a heliostat is made stationary for as long as it takes to obtain the required amount of samples, after which its normal vector is calculated. This will still improve the required time for a full field calibration from three weeks to a few minutes. Another application of the system is the localisation of any object within the heliostat field by simply fixing one of the electromagnetic receivers to the object, provided that it can remain stationary long enough to obtain the required number of samples.

Although the results in this paper are only simulated, they indicate that a tracking error of one milliradian or less is theoretically achievable which is promising enough for the method to merit further investigation. Future work includes verifying the simulated results with laboratory experiments

leading up to field measurements.

## Acknowledgements

Johann Treurnicht, for sharing his invaluable insights and experience, and for his gracious assistance with administration, particularly with regards to finances.

Herman Engelbrecht, for his invaluable insights in all things signal processing, and his willingness to take over the role of lead supervisor halfway through the work.

Everyone else, particularly the people at STERG, who contributed in some way or another.

My Lord and Saviour Jesus Christ for his faithfulness and provision. The fear of the Lord is the beginning of wisdom, and the knowledge of the holy is understanding.

## References

- [1] Gregory J. Kolb et al., "Power Tower Technology Roadmap and Cost Reduction Plan," Sandia National Laboratories, Tech. rep. April 2011.
- [2] J. Ignacio Ortega, J. Ignacio Burgaleta, and Félix M. Téllez, "Central Receiver System Solar Power Plant Using Molten Salt as Heat Transfer Fluid," *Journal of Solar Energy Engineering*, vol. 130, no. 2, February 2008.
- [3] Gregory J. Kolb et al., "Heliostat Cost Reduction Study," Sandia National Laboratories, Tech. rep. June 2007.
- [4] Abraham Kribus et al., "Closed loop control of heliostats," *Energy*, vol. 29, pp. 905-913, 2004.
- [5] Andreas Pfahl, Reiner Buck, and Karsten Rehschuh, "Method for controlling the alignment of a heliostat with respect to a receiver, heliostat device and solar power plant," October 2009.
- [6] Thomas Roos et al., "A 25m2 target-aligned heliostat with closed-loop control," , 2007.
- [7] Mark R. Convery, "Closed-loop control for power tower heliostats," in *Proceedings of SPIE*, vol. 8108, 2011.
- [8] M. Berenguel et al., "An artificial vision-based control system for automatic heliostat positioning offset correction in a central receiver solar power plant," *Science Direct*, vol. 76, pp. 563-575, December 2004.
- [9] Raed Sherif, "Concentrating Solar Power Technologies," in *iNEMI Alternative Energy Workshop*, San Jose, California, October 2010.
- [10] M. Zavodny et al., "Tower-based CSP artificial light calibration system," *Energy Procedia*, vol. 69, pp. 1488-1497, May 2015.
- [11] Kenneth W. Stone and Scott A. Jones, "Analysis of solar two heliostat tracking error sources," Sandia National Laboratories, Tech. rep. 1999.
- [12] William S. Murphy, "Determination of a Position using Approximate Distances and Trilateration," Colorado School of Mines, Master's thesis July 2007.